Artificial
Organs

Thoughts and Progress

A Sliding Mode-Based Starling-Like Controller for Implantable Rotary Blood Pumps

*Mohsen A. Bakouri, †‡Robert F. Salamonsen, *Andrey V. Savkin, §Abdul-Hakeem H. AlOmari, ¶Einly Lim, and **Nigel H. Lovell
*School of Electrical Engineering and Telecommunications; **Graduate School of Biomedical Engineering, University of New South Wales; §Cardiac Technology Centre, Royal North Shore Hospital, Sydney Medical School, The University of Sydney, Sydney, New South Wales; †Department of Epidemiology and Preventive Medicine, Monash University; ‡Department of Intensive Care, Alfred Hospital, Melbourne, Victoria, Australia; and ¶Department of Biomedical Engineering, University of Malaya, Kuala Lumpur, Malaysia

Abstract: Clinically adequate implementation of physiological control of a rotary left ventricular assist device requires a sophisticated technique such as the recently proposed method based on the Frank–Starling mechanism. In this mechanism, the stroke volume of the heart increases in response to an increase in the volume of blood filling the left ventricle at the end of diastole. To emulate this process, changes in pump speed need to automatically regulate pump flow to ensure that the combined output of the left ventricle and pump match the output of the right ventricle across changing cardiovascular states. In this approach, we exploit the linear relationship between estimated mean pump flow $(\bar{Q}_{est})$ and pump flow pulsatility (PI_{Q_p}) in a tracking control algorithm based on sliding mode control. The immediate response of the controller was assessed using a lumped parameter model of the cardiovascular system (CVS) and pump from which could be extracted both $\bar{Q}_{est}$ and PI_{Q_p}. Two different perturbations from the resting state in the presence of left ventricular failure were tested. The first was blood loss requiring a reduction in pump flow to match the reduced output from the right ventricle and to avoid the complication of ventricular suction. The second was exercise, requiring an increase in pump flow. The sliding mode controller induced the required changes in Q_p within approximately five heart beats in the blood loss simulation and eight heart beats in the exercise simulation without clinically significant transients or steady-state errors. **Key Words:** Heart failure—Left ventricular assist device—Starling-like controller—Sliding mode control.

Nowadays, a wide range of therapies has been developed to manage heart failure (HF). These include surgery, drug therapy, and mechanical cardiac assist devices (1,2). As a large percentage of HF is attributed to left ventricular (LV) failure, an implantable left ventricular assist device (LVAD) has emerged as an option to support HF patients in the last decade (3). The continued development of LVADs has seen the emergence smaller, fully implantable rotary blood pumps (IRBPs).

Recently, a review of physiological control mechanisms by AlOmari et al. (4) indicates that no fewer than 30 novel approaches to this problem have been proposed over the past few years. However, none have achieved widespread acceptance by the medical profession. To fill this hiatus, we propose a new approach combining a Starling-like control strategy that is intuitively understood by medical staff (5) with a sliding mode controller (SMC) (6) to determine the physiologically optimum pump flow and calculate the appropriate speed to achieve it. The Starling mechanism emulates the natural processes in the heart to synchronize the outputs of left and right ventricles and to match the pump output to the fluctuating metabolic requirements of the body. In this way, the technique avoids overpumping leading ultimately to ventricular collapse and under pumping, which can cause LV insufficiency (7). SMC combines a rapid response of pump speed without significant overshoot and with high tolerance to noisy reference signals.

The SMC is proposed in order to improve adaptability to cardiac demand and clinical conditions of the heart that have plagued traditional control strategies (8). This modality has proven to be robust in various applications, as its development in the 1950s (6). In this study, a novel SMC is developed to noninvasively regulate the flow error to a set point without inducing suction in the ventricle. A steady-state Kalman estimator (9) was applied to estimate

doi:10.1111/aor.12223

Received June 2013; revised August 2013.

Address correspondence and reprint requests to Mr. Mohsen A. Bakouri, School of Electrical Engineering and Telecommunications, University of New South Wales, Sydney, NSW 2036, Australia. E-mail: m.bakouri@student.unsw.edu.au; mohsenalkhilani@yahoo.co.uk

the system states despite system disturbance and measurement noise. Finally, computer simulations were performed to verify the performance of the proposed controller.

METHODS

Control strategy

According to the Frank–Starling mechanism, an increased volume of blood progressively stretches the ventricular wall, causing the cardiac muscle to contract more forcefully. This mechanism underlies the sigmoid relationship between preload and output of the left ventricle as described by Guyton and Hall (10). Early clinical experience with patients with IRBP established that the relationship between flow pulsatility and LV preload was similarly sigmoid (RF Salamonsen private communication). Thus, when LV output is related to flow pulsatility the relationship approaches linearity. The theoretical basis for this has been presented in detail elsewhere (5). Recently, our research group has developed and validated a numerical approach that uses pulsatility to control pump flow in a manner that emulates the starling mechanism of the natural heart. When changes in state occur (Fig. 1), they cause deviations of the operating point from its original position on the control line, for example, to state-lines S2 or S3. The disposition of the states S1, S2, and S3 conform to our previously reported theoretical analysis (5). The controller then forces the operating point back to the control line along a radial path as defined by Eq. 1, that is:

$$\bar{Q}_{pr} = \left(\sqrt{(\bar{Q}_{est})^2 + (PI_{Q_p})^2}\right) * \sin\theta_n \qquad (1)$$

where $\bar{Q}_{pr}$ is the desired pump flow, $\bar{Q}_{est}$ is the estimated mean pump flow, PI_{Q_p} is pulsatility of pump flow, and θ_n is the angle that defines pump assist ratio. A radial correction is used as it conforms closely to the trajectories of the new state lines S2 or S3. Changes in state are thus countered by movements of the operating point up or down the control line. The pump flow defined by each new location of the operating point on the control line is the value to be used for the next cardiac cycle of the model.

Flow estimator method

Our research group has developed a noninvasive empirical model of an LVAD to estimate mean flow $\bar{Q}_{est}$ (11). In this model, two autoregressive dynamical linear time-variant (ARX) models were used. The first ARX model is proposed to model the relation between mean pulsatility index of pump rotational speed $(\overline{PI}_w)$ and mean pulse-width modulation signal $(\overline{PWM})$ as follows:

$$\hat{x}_1(k+1) + \sum_{i=1}^{n} a_i(k-i+1)\hat{x}_1(k-i+1) = \sum_{j=1}^{m} b_j(k-j+1)u(k-j-q_1+1) + e_1(k) \qquad (2)$$

where $\hat{x}_1$ is the estimated mean pulsatility index of pump rotational speed $\overline{PI}_\omega$, $\underline{u(k)}$ is the mean pulse-width modulation signal $\overline{PWM}$, $a(k)$, $b(k)$ are the output and input time-varying system parameters respectively, $e_1(k)$ is the model noise, q_1 is the delay value, k is the sampling time, and n and m represent the model output and input orders, respectively.

Similarly, the second ARX model is proposed to model the relation between $\bar{Q}_{est}$ and $\overline{PI}_\omega$ as follows:

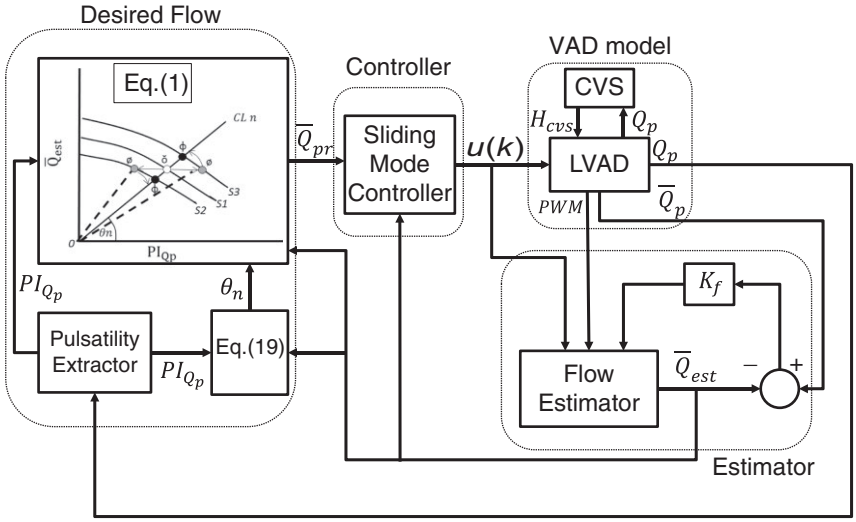

FIG. 1. Block diagram of control system. $\bar{Q}_p$, Average pump flow, PI_{Qp}, pulsatility of pump flow; CLn, nth Control line; (θ_n), angle defining the slope of the nth control line; S1, original state; S2 & S3, deviated states; ŏ, original position of operating point; ø, deviated position of operating point caused by the change in state; ϕ position of operating point after action of controller; $\bar{Q}_{pr}$, the reference (desired) mean pump flow; LVAD, left ventricular assist device; $u(k)$, pulse-width modulation drive signal to the LVAD; H_{cvs}, differential pressure between left ventricular and aortic pressure; CVS, model of the cardiovascular system; Q_p, instantaneous pump flow; $\bar{Q}_p$, mean pump flow; $\bar{Q}_{est}$, estimated mean flow; K_f, Kalman gain.

$$\hat{x}_2(k+1)+\sum_{i=1}^{n} c_i(k-i+1)\,\hat{x}_2(k-i+1) = \sum_{j=1}^{m} d_j(k-j+1)\,\hat{x}_1(k-j-q_2+1)+e_2(k) \quad (3)$$

where $\hat{x}_1$ is the estimated $\overline{\mathrm{PI}}_\omega$, $\hat{x}_2$ is the estimated $\overline{\mathrm{Q}}_{est}$, $c(k)$, $d(k)$ are the output and input time-varying system parameters, respectively, $e_2(k)$ is the model noise, q_2 is the delay value, k is the sampling time, and n and m represent the model output and input orders, respectively.

This approach used a recursive least square method to estimate the system parameters. In both ARX models, the constant forgetting factor method was used to track the time varying parameters online. This method was chosen because it is accommodated the law variation changes due to change of afterload, preload, and contractility. Therefore, fast tracking of system parameters to sudden changes of venous return will achieved, for example, from changes of body posture or straining (12). In both models the best results (i.e., with minimal error and highest correlation values between the estimated and measured values of $\overline{\mathrm{PI}}_\omega$ and $\overline{\mathrm{Q}}_{est}$) were obtained when the system orders were $n = m = 1$, and the delay values were $q_1 = q_2 = 1$. Therefore, the dynamic model of the system can be described by the following difference equations as:

$$\hat{x}_1(k+1)+a(k)\,\hat{x}_1(k) = b(k)u(k)+e_1(k) \quad (4)$$

$$\hat{x}_2(k+1)+c(k)\,\hat{x}_2(k) = d(k)x_1(k)+e_2(k) \quad (5)$$

where $x_1(k)$ is the estimated $\overline{\mathrm{PI}}_\omega$, $x_1(k)$ is the estimated $\overline{\mathrm{Q}}_{est}$, $u(k)$ is the $\overline{\mathrm{PWM}}$, $a(k)$, $b(k)$, $c(k)$ and $d(k)$ are time-varying system parameters, and $e_1(k)$, $e_2(k)$ are the model noises. In this model, different cardiovascular states are simulated by using different values of hemodynamic parameters including; total blood volume (V_{total}), systemic vascular resistance (R_{sa}), and parameters representing the LV contractility (E_{lv}).

In order to design a physiological controller, the system defined by Eqs. 4 and 5 is rearranged as a linear time-variant state space system of the form:

$$\begin{aligned} x(k+1) &= A(k)x(k)+B(k)u(k)+\zeta(k) \\ y(k) &= Cx(k) \end{aligned} \quad (6)$$

where, $A(k)=\begin{bmatrix} -a(k) & 0 \\ d(k) & -c(k) \end{bmatrix}$, $B=\begin{bmatrix} b(k) \\ 0 \end{bmatrix}$ and $C = [0\ 1]$ where, $x(k) = [x_1(k)\ x_2(k)]$, $\zeta(k)$ is the system noise, $y(k)$ is the system output, $a(k)$, $b(k)$, $c(k)$, and $d(k)$ are the system parameters estimated using an identification algorithm. In this model, experimental results showed that the variation of $a(k)$, $c(k)$, and $d(k)$ are bounded and the parameter $b(k)$ is close to a constant value.

Implementation of SMC algorithm

We can re-write the state space model (6) as:

$$\begin{aligned} x(k+1) &= Ax(k)+\delta Ax(k)+Bu(k)+\zeta(k) \\ y(k) &= Cx(k) \end{aligned} \quad (7)$$

where δA is the system parameter variation and $\zeta(k)$ is the system disturbance.

In this strategy, the controller was designed based on SMC using a pole placement method (13). In this technique, the control system matrix is given by $(A - BK)$. Here $k \in R^n$ is the gain matrix obtained by assigning n-desired eigenvalues in the pole placement. To accommodate a strong reachability, we propose the Gao reaching law (14). This law can be given as:

$$s(k+1) = (1-qT)s(k)-\varepsilon T\mathrm{sign}(s(k)) \quad (8)$$

where, $T > 0$ is the sampling period, $\varepsilon > 0$, $q \geq 0$ such that $0 < (1 - qT) < 1$.

We define the sliding surface as:

$$s(k) = Sx(k) \quad (9)$$

where S is a constant vector, designed using the method described in (15) to ensure that $x(k)$ is asymptotically stable. To satisfy the reaching law in Eq. 8, we obtain:

$$s(k+1) = Sx(k+1) \quad (10)$$

From Eqs. 7 and 10 we get:

$$\begin{aligned} s(k+1) &= Sx(k+1) \\ &= S((A-BK)x(k)+\delta Ax(k)+Bu(k)+\zeta(k)) \end{aligned} \quad (11)$$

Equations 8 and 11 give:

$$\begin{aligned} &S((A-BK)x(k)+\delta Ax(k)+Bu(k)+\zeta(k)) \\ &= (1-qT)s(k)-\varepsilon T\mathrm{sign}(s(k)) \end{aligned} \quad (12)$$

Solving the above equation for the control command signal u(k) yields:

$$\begin{aligned} u(k) = -(SB)^{-1}(&S(A-BK)x(k)+S\delta Ax(k)+ \\ &S\zeta(k)+(qT-1)Sx(k)+\varepsilon T\mathrm{sign}(s(k))) \end{aligned} \quad (13)$$

As δA and $\zeta(k)$ are unknown, the control law cannot be implemented unless we assume that the upper and lower bounds of the value $(S\delta Ax(k) + S\zeta(k))$ is given as:

$$-zT < S\delta Ax(k) + S\zeta(k) < zT \quad (14)$$

then the control law can be rewritten as:

$$u(k) = -(SB)^{-1}(S(A-BK)x(k) + z\mathrm{Tsign}(s(k)) + (qT-1)Sx(k) + \varepsilon\mathrm{Tsign}(s(k))) \quad (15)$$

In our problem, the whole state $x(k)$ is not available to our controller, so we need to estimate $x(k)$ based on the measured output $y(k)$. For this purpose, we use the steady-state Kalman estimator as described in (9). So, the Kalman estimator can be written as:

$$\hat{x}(k+1) = A\hat{x}(k) + Bu(k) + K_f(y(k) - C\hat{x}(k)). \quad (16)$$

Here $\hat{x}(k)$ is the estimate of the state $x(k)$ and K_f is the optimal Kalman gain given as:

$$K_f = PC^T R^{-1} \quad (17)$$

where P is the solution of the algebraic Riccati equation:

$$AP + PA^T - PC^T R^{-1} CP + Q = 0 \quad (18)$$

In our control design, we have applied the control law in Eq. 15 with the state $x(k)$ replaced by its estimated $\hat{x}(k)$.

As shown in Fig. 1, the desired reference pump flow $\bar{Q}_{pr}$ was calculated using gradient angle (θ) of the control line as:

$$\theta = K_{p,\theta}\left(e_{\bar{Q}_{est}} + e_{PI(Q_p)}\right) + K_{i,\theta}\int\left(e_{\bar{Q}_{est}} + e_{PI(Q_p)}\right) \quad (19)$$

where K_p and K_i are the proportional and integral gains. This proportional integral controller ensures that the gradient angle θ is automatically adjusted to insure that $\bar{Q}_{est}$ and PI_{Q_p} remain within their corresponding upper and lower limits for each cycle of the model. Therefore, the reference pump flow can be given as stated in Eq. 1.

Simulation protocols

Numerical simulations using a software model incorporating a lumped-parameter model of the CVS in combination with a model of the RBP was used to evaluate the control strategy. These were implemented using Matlab-Simulink (The Math-works Inc., Natick, MA, USA). A detailed description of the model as well as parameter values, previously developed by our research group, can be obtained from (16). In order to evaluate the immediate response of the controller to different physiological states, defined by system parameter variations, the LVAD with the designed controller was tested under two physiological conditions. First, V_{total} was linearly decreased by 500 mL at 25 s, and the simulation was continued for another 35 s to allow the system to reach a steady state corresponding to new parameters values. Next, we simulated the transition from rest to exercise. In this test, the system parameters were also linearly changed at 25 s. These changes include E_{lv} and right ventricular contractility (E_{rv}) (increased by 15%), R_{sa} (decreased by 50%) and systemic veins unstressed volume ($V_{0,sv}$) (decreased by 50%). This test was conducted to determine whether the controller had the capacity in combination with the CVS to provide the hemodynamic support required during normal daily activities. The other parameters of the model did not change through the simulation study.

The design parameters of the sliding surface in Eq. 15 were S = [0.9413 – 0.0805] and those of the control law in the same equation were $qT = 0.01$ and $\varepsilon T = 0.02$. Also, the resulting value of S is [0.9413 – 0.0805]. In addition, the lower and upper limits for pump flow pulsatility were set to 1.5 and 4 L/min, whereas lower and upper limits for mean pump flow were set to 3 and 6 L/min. Study protocol model parameters were adjusted from the "Healthy" to "Heart failure" condition as a precondition for simulations. The most parameters including systemic peripheral resistance, blood volume, and contractilities of the left and right ventricles expressed as maximum end-diastolic elastances are given in Table 1.

RESULTS

Figure 2 (A series) shows the immediate response of the controller to blood loss occurring at 25 s. The reduction in blood volume caused a fall in RV preload and consequent delivery of blood to the LV, which in turn reduced LV preload and stroke work. The controller responds to the consequent fall in pump flow pulsatility by decreasing mean pump speed from 2800 rpm to 2000 rpm and mean pump flow from 4.6 L/min to 3.4 L/min. These changes were substantially complete within four heartbeats. Figure 2, A2 giving a magnified view of the relationship between actual and estimated instantaneous pump flows, indicate the extremely close correlation between the two flows. The relationship between actual and estimated average flows was highly significant (Fig. 2, A3) and linear regression gave an $R^2 = 0.9999$ and a slope of unity.

In the second scenario, model parameters were changed to simulate the transition from rest to exer-

TABLE 1. *Changes in important model parameters to simulate the "heart failure" condition*

No.	Variable	Unit	Heart failure	(Healthy)
1	R_{sa}	mm Hg.s/mL	1.11	(0.74)
2	V_{total}	mL	5800	(5300)
3	$E_{\max,lv}$	mm Hg/mL	0.71	(3.54)
4	$E_{\max,rv}$	mm Hg/mL	0.53	(1.74)

R_{sa}, Resistance of systemic arteries; V_{total}, total blood volume; $E_{\max,lv}$, maximum end-systolic elastance of the LV; $E_{\max,rv}$, maximum end-systolic elastance of the RV. Reference values for the "Healthy" condition are given in brackets.

cise. Figure 2, B series, illustrates the immediate response of the controller to the parameter changes occurring at 25 s. The controller responds to an increase in LV preload, stroke work, and subsequent pump flow pulsatility by increasing mean pump speed from 2800 rpm to 3300 rpm and mean pump flow from 4.4 L/min to 5.1 L/min. These changes were substantially complete within eight heartbeats without transient overshoots or steady state errors. As for the previous example, Fig. 2, B2 shows actual and estimated instantaneous pump flows, whereas Fig. 2, B3 demonstrates the extremely high value of 0.9998 for R^2, and a slope of unity.

Table 2 presents a summary of salient hemodynamic variables, specific for the HF condition, before and after perturbations of blood loss and exercise.

DISCUSSION

This study demonstrates for the first time the application of the SMC technique to the recently described Starling-like controller (5) for physiological control of pump speed in an IRBP. In the two simulations presented that cover both perturbations in blood volume and exercise resulting in decreases

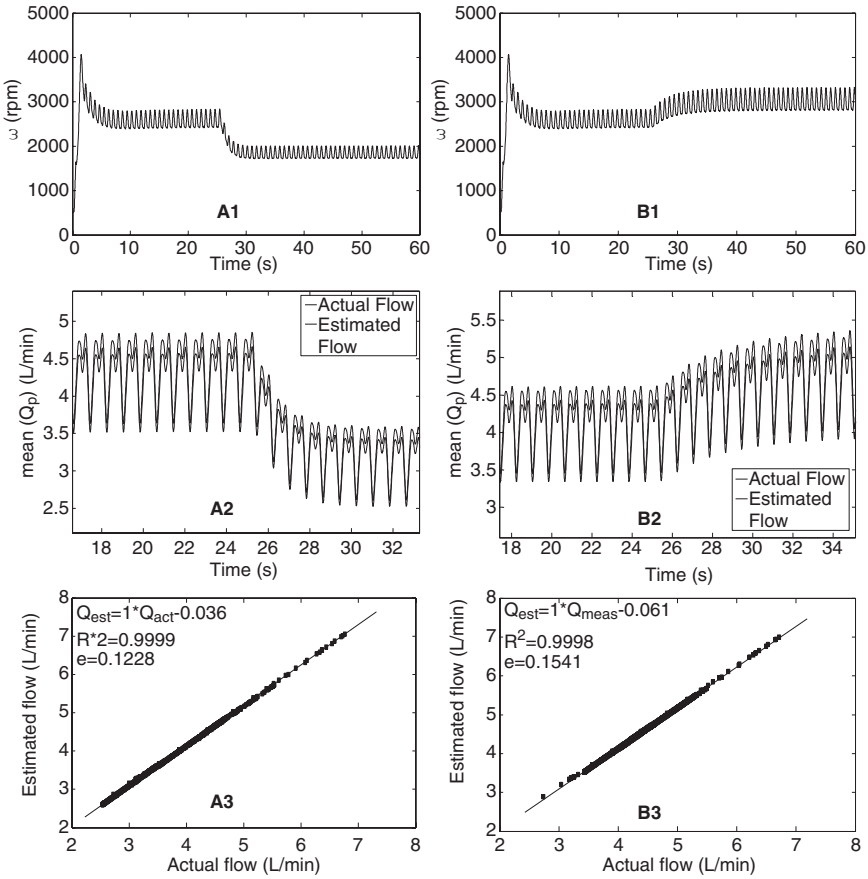

FIG. 2. System and controller response to perturbations of the circulation. A series, Blood loss, A1, pump speed; A2, Magnified view of estimated versus actual pulsatile pump flow; A3 estimated versus actual steady-state blood flow. B series, Exercise; B1 Pump speed; B2 Magnified view of estimated versus actual pulsatile pump flow; B3, estimated versus actual steady state blood flow; Q_p, pump flow; ω, pump speed.

TABLE 2. *Associated hemodynamic variables at rest and in test conditions*

		Heart failure plus LVAD		
Variable	Unit	Rest	Blood loss	Exercise
P_{lved}	mm Hg	10.4	6.5	21.5
P_{rved}	mm Hg	7.8	5.2	13.9
V_{lves}	L/min	38.8	62.7	54.1
V_{lved}	L/min	142.7	132.3	152.4
SV	mL	100.0	96.7	100.0
$\bar{P}_{ao}$	mm Hg	83.5	97.8	125.1

P_{lved}, LV end diastolic pressure; P_{rved}, RV end diastolic pressure; V_{lves}, LV end systolic volume; V_{lved}, LV end diastolic volume; SV, stroke volume; mean; $\bar{P}_{ao}$, mean aortic pressure.

and increases in pump speed, respectively, appropriate changes in pump speed and flow were induced extremely rapidly without significant transient or steady state error. In the field of physiological control, our argument is that the Starling-like controller, which emulates the inherent control mechanism in the natural heart to synchronize the outputs of left and right ventricles, is superior to other reported physiological strategies. These include control of differential pressure across the pump (8); afterload control (17); flow control (18); preload control (19); and control of pulsatility gradient (20). In the healthy cardiovascular system, the cardiac output is generated ultimately not by the left ventricle but by the metabolic requirements of the tissues as transferred to the left heart by the right heart via the pulmonary circulation (1). In this context, the ultimate control goal of the LVAD should therefore be to maintain a stable appropriate level of work for the failing left ventricle and at the same time deliver the output from the pulmonary circulation to the arterial compartment. If it achieves this aim it should ensure a mean arterial pressure in excess of 60 mm Hg, which is a fundamental prerequirement for autoregulation of flows by the tissues (21).

The second important prerequisite for any control system particularly at low preloads where there is an imminent risk of ventricular suction is a rapid speed of response as the starling effect in ventricular muscle is virtually immediate. Some physiological events like changes in posture can cause ventricular suction within 10 heart beats. The sliding mode controller meets this requirement very competently. Our simulations indicate that the response time for change in pump speed is five to eight heartbeats. In this respect, it is superior to standard proportional-integral-derivative controllers where the high gain for the proportional coefficient necessary for a rapid response leads to under damped transient responses, which result in overshoots and oscillations in pump speed (9). In addition, the operation of the derivative component, designed to control this problem, is compromised by the noisy nature of estimated flow and flow pulsatility signals. Other advantages of SMC in addition to speed of response include zero steady state error, robustness in face of large perturbations or model uncertainties, successful application to nonlinear systems, and reduced requirements for information in contrast to classical systems. An additional attraction of the technique is its simplicity and ease of implementation (6).

The Starling-like controller also requires accurate data on pump speed and speed pulsatility, which in this communication are estimated. Although estimation avoid the problems inherent in flow and pressure sensors, they introduce problems of their own—most importantly inaccuracy and slow speeds of operation, because a number of heart beats are required for each estimation (22).

One limitation of the method is that it is dependent on a moderate degree of residual LV contractility and will not work in the extreme case where LV has no contractility at all. Furthermore, Fig. 2, A1 and B1 indicate that the transient overshoot to 7 L/min occurs at the beginning of the simulation before a steady state is achieved. Further tuning of the controller is required to eliminate this problem (23,24).

CONCLUSION

In this paper we present a new physiological controller that mimics the Frank–Starling law of the heart and that includes a novel robust optimal SMC. The controller adjusts mean pulsatile flow using pump flow pulsatility as the feedback parameter. The immediate response of the controller to changes in rest and changes from rest to exercise that impose very different operating conditions for the controller were evaluated using a lumped parameter model of the cardiovascular system. Simulation results show that the abnormal hemodynamic variables of HF patients are restored back to a normal physiological range. Future work will include the validation of the proposed strategy using a circulation mock loop and in vivo animal experiments.

REFERENCES

1. Birks EJ, Tansley PD, Hardy J, et al. Left ventricular assist device and drug therapy for the reversal of heart failure. *N Engl J Med* 2006;355:1873–84.
2. Stevenson LW, Miller LW, Desvigne-Nickens P, et al. Left ventricular assist device as destination for patients undergoing intravenous inotropic therapy. A subset analysis From REMATCH (randomized evaluation of mechanical assistance

in treatment of chronic heart failure). *Circulation* 2004;110: 975–81.
3. Nosé Y, Yoshikawa M, Murabayashi S, Takano T. Development of rotary blood pump technology: past, present, and future. *Artif Organs* 2000;24:412–20.
4. AlOmari AH, Savkin AV, Stevens M, et al. Developments in control systems for rotary left ventricular assist devices for heart failure patients: a review. *Physiol Meas* 2013;34:R1–27.
5. Salamonsen RF, Lim E, Gaddum N, et al. Theoretical foundations of a Starling-like controller for rotary blood pumps. *Artif Organs* 2012;36:787–96.
6. Utkin VI. Scope of the theory of sliding modes. In: Dickinson BW, Fettweis A, Massey JL, Modestino JW, Sontag ED, Thoma M, eds. *Sliding Modes in Control and Optimization*. Berlin: Springer-Verlag, 1992;116.
7. Hall AW, Soykan O, Harken AH. Physiologic control of cardiac assist devices. *Artif Organs* 2008;20:271–5.
8. Bullister E, Reich S, Sluetz J. Physiologic control algorithms for rotary blood pumps using pressure sensor input. *Artif Organs* 2002;26:931–8.
9. Goodwin GC, Graebe SF, Salgado ME. Design via optimal control techniques. In: Goodwin et al., eds. *Control System Design*. Upper Saddle River, NJ: Prentice Hall, 2001;240.
10. Guyton AC, Hall JE. *Textbook of Medical Physiology*. Philadelphia, PA: Elsevier Saunders, 2006.
11. AlOmari AH, Javed F, Savkin AV, et al. Non-invasive measurements based model predictive control of pulsatile flow in an implantable rotary blood pump for heart failure patients. *Conference Proceeding IEEE Mediterranean of Control and Automation*. 2011;491–6.
12. Arndt A, Nüsser P, Graichen K, Müller J, Lampe B. Physiological control of a rotary blood pump with selectable therapeutic options: control of pulsatility gradient. *Artif Organs* 2008;32:761–71.
13. Edwards C, Spurgeon S. Sliding mode design approaches. In: Reilly OJ, Rogers E, ed. *Sliding Mode Control: Theory and Applications*. Boca Raton, FL: CRC Press, 1998;7.
14. Gao W, Wang Y, Homaifa A. Discrete-time variable structure control systems. *IEEE Trans Ind Electron* 1995;42:117–22.
15. Spurgeon SK. Hyperplane design techniques for discrete-time variable structure control systems. *Int J Control* 1992;55:445–56.
16. Lim E, Dokos S, Cloherty SL, et al. Parameter-optimized model of cardiovascular–rotary blood pump interactions. *IEEE Trans Biomed Eng* 2010;57:254–66.
17. Wu Y, Paul A, Tao G, Wood H, Olsen D, Tribble C. An advanced physiological controller design for a left ventricular assist device to prevent left ventricular collapse. *Artif Organs* 2003;27:926–30.
18. Lim E, AlOmari AH, Savkin AV, et al. A method for control of an implantable rotary blood pump for heart failure patients using non-invasive measurements. *Artif Organs* 2011;35:E174–80.
19. Choi S, Antaki JE, Boston R, Thomas D. A sensorless approach to control of a turbodynamic left ventricular assist system. *IEEE Trans Control Syst Technol* 2001;3:473–82.
20. Choi S, Boston JR, Antaki JF. Hemodynamic controller for left ventricular assist device based on pulsatility ratio. *Artif Organs* 2007;31:114–25.
21. McIntyre KM, Sasahara AA. The hemodynamic response to pulmonary embolism in patients without prior cardiopulmonary disease. *Am J Cardiol* 1971;28:288–94.
22. Slaughter MS, Bartoli CR, Sobieski MA, et al. Intraoperative evaluation of the Heartmate II flow estimator. *J Heart Lung Transplant* 2009;28:39–43.
23. Petersen IR, Ugrinovskii VA, Savkin AV. *Robust Control Design Using H-infinity Methods*. London: Springer-Verlag, 2000.
24. Savkin AV, Evans RJ. *Hybrid Dynamical Systems. Controller and Sensor Switching Problems*. Boston, MA: Birkhauser, 2002.

Acoustic Analysis of a Mechanical Circulatory Support

*‡Laila Hubbert, *‡Per Sundbom, §Matthias Loebe, †‡Bengt Peterzén, †‡Hans Granfeldt, and †‡Henrik Ahn
*Clinical Department of Cardiology at the Heart Center, University Hospital of Linkoping; †Department of Cardiovascular Surgery and Anesthesia at the Heart Center, University Hospital of Linkoping; ‡Department of Medicine & Health, Linkoping University, Linkoping, Sweden; and §Division of Transplant and Assist Devices at Methodist DeBakey Heart & Vascular Center, Houston, TX, USA

Abstract: Mechanical circulatory support technology is continually improving. However, adverse complications do occur with devastating consequences, for example, pump thrombosis that may develop in several parts of the pump system. The aim of this study was to design an experimental clot/thrombosis model to register and analyze acoustic signals from the left ventricular assist device (LVAD) HeartMate II (HMII) (Thoratec Corporation, Inc., Pleasanton, CA, USA) and detect changes in sound signals correlating to clots in the inflow, outflow, and pump housing. Using modern telecom techniques, it was possible to register and analyze the HMII pump-specific acoustic fingerprint in an experimental model of LVAD support using a mock loop. Increase in pump speed significantly ($P < 0.005$) changed the acoustic fingerprint at certain frequency (0–23 000 Hz) intervals (regions: R1–3 and peaks: P1,3–4). When the ball valves connected to the tubing were narrowed sequentially by ~50% of the inner diameter (to mimic clot in the out- and inflow tubing), the frequency spectrum changed significantly ($P < 0.005$) in P1 and P2 and R1 when the outflow tubing was narrowed. This change was not seen to the same extent when the lumen of the ball valve connected to the inflow tube was narrowed by ~50%. More significant ($P < 0.005$) acoustic changes were detected in P1 and P2 and R1 and R3, with the largest dB figs. in the lower frequency ranges in R1 and P2, when artificial clots and blood clots passed through the pump system. At higher frequencies, a significant change in dB figs. in R3 and P4 was detected when clots passed through the pump system. Acoustic monitoring

doi:10.1111/aor.12244

Received July 2013; revised September 2013.

Corresponding Author: Dr. Laila Hubbert, Department of Cardiology at the Heart Center, University Hospital—Departments of Medicine & Health, Linkoping University, Linkoping 581 85, Sweden. E-mail: Laila.Hubbert@lio.se